1 **Title**

2 ***Drosophila Bchs* overexpression recapitulates human *WDFY3* neurodevelopmental**
3 **phenotypes with implications for glial cell involvement in altered head circumference**

4

5 **Authors**

6 Marek B. Körner[1,2#], Akhil Velluva[1], Linnaeus Bundalian[1], Knut Krohn[3], Kathleen Schön[3],
7 Isabell Schumann[1], Jessica Kromp[1,4], Andreas S. Thum[4], Antje Garten[5], Julia Hentschel[1], Rami
8 Abou Jamra[1], Achmed Mrestani[2,6], Nicole Scholz[2], Tobias Langenhan[2], Diana Le Duc[1,7#]

9

10

11 **Affiliations**

12 [1] Institute of Human Genetics, University of Leipzig Medical Center, 04103 Leipzig, Germany

13 [2] Rudolf Schönheimer Institute of Biochemistry, Division of General Biochemistry, Leipzig
14 University, Johannisallee 30, 04103 Leipzig, Germany

15 [3] Core Unit DNA-Technologies, Medical Faculty, Leipzig University, Philipp-Rosenthal-Str.
16 55, 04103 Leipzig, Germany

17 [4] Department of Genetics, Institute of Biology, Leipzig University, Talstraße 33, 04103 Leipzig,
18 Germany

19 [5] Pediatric Research Center, University Hospital for Children and Adolescents, Leipzig
20 University, 04103 Leipzig, Germany

21 [6] Department of Neurology, University of Leipzig Medical Center, 04103 Leipzig, Germany

22 [7] Department of Evolutionary Genetics, Max Planck Institute for Evolutionary Anthropology,
23 04103, Leipzig, Germany

24

25 [#] Correspondence to Gabriela-Diana.LeDuc@medizin.uni-leipzig.de and
26 marek.koerner@medizin.uni-leipzig.de

27

Abstract

The autophagy adaptor *WDFY3* is linked to neurodevelopmental delay and altered brain size. Loss-of-function variants are associated with an increased brain size in both humans and mice. We thus, hypothesized that the microcephaly observed in some of the patients may be related to a gain-of-function of the *WDFY3* gene product. While the role of *WDFY3* loss-of-function has been studied extensively in neurons, little is known about the effects of *WDFY3* overexpression in different neural cell types. We utilized a *Drosophila melanogaster* overexpression model to investigate the effect of the *WDFY3* ortholog *Bchs* (*blue cheese*) on development, CNS size, and gene expression profiles. Glial and neuronal overexpression of *Bchs* impaired CNS development, locomotion and autophagy. Glial overexpression of *Bchs* also altered CNS size significantly. We identified 79 genes that were differentially expressed and overlapped in flies that overexpress *Bchs* in glial and neuronal cells, respectively. Additionally, upon neuronal *Bchs* overexpression differentially expressed genes clustered in gene ontology categories associated with autophagy and mitochondria. Our data indicate that *WDFY3*/*Bchs* overexpression in both neurons and glial cells results in impaired neural development, which corresponds to symptoms observed in *WDFY3*-related neurodevelopmental delay.

Keywords: *WDFY3*, ALFY, *Bchs*, neurodevelopmental delay, transcriptomics

Introduction

Over the past decade, a growing body of evidence, including functional analyses and patient related data, has provided substantial support for the involvement of *WDFY3* in neurodevelopmental disorders (Le Duc *et al.* 2019; Stessman *et al.* 2017; Wang *et al.* 2016). *WDFY3* encodes an autophagosomal scaffolding protein involved in targeted recruitment and destruction of macromolecular components including aggregation-prone proteins (Clausen *et al.* 2010; Filimonenko *et al.* 2010; Finley *et al.* 2003; Simonsen *et al.* 2004).

Previous studies in mice demonstrated that *Wdfy3* regulates neurodevelopmental processes such as neuronal connectivity, proliferation, migration, and synaptic morphology (Dragich *et al.* 2016; Orosco *et al.* 2014; Schaaf *et al.* 2022; Søreng *et al.* 2022). Loss-of-function variants of *WDFY3* or its *Drosophila* ortholog *blue cheese* (*Bchs*) result in neurodegeneration and protein aggregation, indicating autophagic defects (Clausen *et al.* 2010; Filimonenko *et al.* 2010; Finley *et al.* 2003; Fox *et al.* 2020; Han *et al.* 2015; Hebbar *et al.* 2015; Lim & Kraut 2009; Simonsen *et al.* 2004). The increased head circumference, but also a decreased learning capacity observed in affected human individuals, were faithfully recapitulated in heterozygotes of a *Wdfy3* knockout mouse model, while homozygotes of hypomorphic *Wdfy3* alleles showed perinatal lethality (Dragich *et al.* 2016; Le Duc *et al.* 2019; Orosco *et al.* 2014). However, while loss-of-function variants were associated with increased head circumference, at least two variants have been identified in individuals with microcephaly (Kadir *et al.* 2016; Le Duc *et al.* 2019). We, thus, hypothesized that *WDFY3* loss- and gain-of-function genotypes may result in opposing phenotypes in respect to brain size.

Currently an increasing number of studies concentrate on loss of *WDFY3*/*Bchs* and its effects on the nervous system with a focus on neuronal impairment. Although glial cells are known to play an essential role for neuronal function and neurodevelopment (Bittern *et al.* 2021; Kim *et al.* 2020; Lago-Baldaia *et al.* 2020; Rahman *et al.* 2022), they have received rather

little attention in the effort to unravel *WDFY3*-associated pathomechanisms. So far, it was shown that loss of *Wdfy3* is accompanied with mislocalisation of glial guidepost cells, which provide guidance cues for the formation of axonal tracts (Dragich *et al.* 2016). Hypomorphic *Wdfy3* alleles also increase symmetric proliferative divisions of radial glial cells, neural stem cells which give rise to neurons and glia (Orosco *et al.* 2014). Further, *Wdfy3* is involved in the turnover of oligodendrocytic myelin sheaths (Aber *et al.* 2022). Single-cell RNA-sequencing (RNA-seq) demonstrated an approximately 10× higher *WDFY3* expression in neurons and glial cells compared to all other cells (nTPM > 200) with oligodendrocytes showing the highest expression (nTPM > 400) (Karlsson *et al.* 2021). Hence, glial cells may play an important role in the pathophysiology of *WDFY3*-related neurodevelopmental disorders.

To address the unknown role of glial cells in *WDFY3*-related pathologies and to understand whether *WDFY3* overexpression as proxy for a *WDFY3* gain-of-function condition may be related to neurodevelopmental disorders, here we investigated the effects of *Bchs* overexpression in glial cells and neurons. While both glial and neuronal *Bchs* overexpression impaired neural development, locomotion, and autophagy, central nervous system (CNS) size was altered only after overexpression in glial cells. Further, based on transcriptomics analyses we identified differentially expressed genes in glial and neuronal *Bchs* overexpression flies compared to the respective controls. We found an overlap of 79 differentially expressed genes in both *Bchs* overexpression conditions, which may be involved in the pathological mechanism that unfolds upon *WDFY3* dysfunction.

Results

Developmental delay in glial Bchs overexpression flies

A common symptom of probands carrying a pathogenic *WDFY3* variant is neurodevelopmental delay (Le Duc *et al.* 2019; Stessman *et al.* 2017; Wang *et al.* 2016). In

flies, both loss-of-function and overexpression of the *WDFY3* ortholog *Bchs* were previously shown to impair neuronal function (Finley *et al.* 2003; Hebbar *et al.* 2015; Khodosh *et al.* 2006; Kraut *et al.* 2001; Kriston-Vizi *et al.* 2011; Lim & Kraut 2009; Sim *et al.* 2019; Stessman *et al.* 2017). However, not much is known about how *Bchs* dysregulation impacts glial cells. To better understand the relevance of *Bchs* in different neural cell types, we tested the effect of *Bchs* overexpression, as a proxy for gain-of-function effects, in glial cells (*repo-Gal4*) and neurons (*nSyb-Gal4*) on development, locomotion, CNS morphology, and autophagy (DiAntonio *et al.* 1993; Sepp *et al.* 2001). We found that panglial *Bchs* overexpression delayed the development from egg to adult fly (Fig 1A). Importantly, Mendelian ratios of the adult F1 generation of crossing *Gal4/Sb* with *UAS-bchs::HA/Sb* for panglial and panneuronal *Bchs* overexpression corresponded to the expected ratios, but ubiquitous *Bchs* overexpression (*act5C-Gal4*) was lethal (Fig S1). The developmental time of neuronal *Bchs* overexpression animals was further investigated to exclude a delay in early developmental steps, which cannot be detected at the stage of adult eclosion. The timepoint of larval hatching was not delayed in animals overexpressing *Bchs* in neurons, indicating normal embryonal development (Fig S2A). However, a significantly reduced size of neuronal *Bchs*-overexpressing larvae was observed in early larval development (62.44 h and 100.8 h after egg laying), but not in later larval stages (153 h after egg laying) (Fig S2B). These data suggest that neuronal *Bchs* overexpression causes changes in development during early larval stages.

Panneuronal *Bchs* overexpression caused deficits in the development of the wings and thorax (Fig 1B,E). Adult flies did not properly expand their wings (~90 %) and displayed a dimpled thorax (~43 %). In contrast, only a small percentage of flies overexpressing *Bchs* in glial cells (wing: ~22 %, thorax: 3 %) presented with those deficits (Fig 1D,E). Crustacean cardioactive peptide (CCAP) neurons are known to play an essential role in wing expansion (Luan *et al.* 2006; Park *et al.* 2003). Therefore, we hypothesized that *Bchs* overexpression in

this subtype of neurons caused the wing and thorax abnormalities. Driving *Bchs* overexpression specifically only in CCAP neurons (*CCAP-Gal4*) resulted in almost complete penetrance of those defects (wing: ~100 %, thorax: ~99 %), as opposed to *Bchs* overexpression in motoneurons (*ok6-Gal4*, wing: ~19 %, thorax: ~1 %)) (Fig S1). Hence, CCAP neurons are sensitive to *Bchs* overexpression.

Since probands with *WDFY3* variants show impaired motor coordination (Le Duc *et al.* 2019), we also tested larval locomotion in our fly models. Both panglial and panneuronal *Bchs* overexpression decreased larval crawling velocities indicating a locomotion deficit (Fig 2C,F). Overexpressing *Bchs* only in the subset of motoneurons (*ok6-Gal4*) was sufficient to slow larval movement (Fig S4). Together these data show that glial and neuronal *Bchs* overexpression impacts fly development and locomotion.

Glial Bchs regulates CNS size and glial cell number

Another symptom in carriers of pathogenic *WDFY3* variants is their abnormal head circumference (Le Duc *et al.* 2019; Stessman *et al.* 2017; Wang *et al.* 2016). It was previously described that the *Bchs* loss-of-function mutant $bchs^{58}$ presents with decreased larval and adult brain volumes, while neuronal *Bchs* overexpression by *elav-Gal4* causes an increased larval brain volume (Finley *et al.* 2003; Kriston-Vizi *et al.* 2011). Further, fly pharates ubiquitously overexpressing human *WDFY3* carrying a missense variant that is linked to microcephaly in human individuals, displayed smaller brain volumes (Kadir *et al.* 2016).

In our setup, neuronal *Bchs* overexpression did not alter the brain size to fly length ratio in adult flies or the ventral nerve cord (VNC) length in larvae and adults (Fig 2E,3E,F). However, we found that adult flies overexpressing *Bchs* in glial cells had a decreased brain size to fly length ratio (Fig 3B), while neither brain size nor fly length alone were significantly altered in comparison to controls (Fig S5A,B). Further, glial *Bchs* overexpression markedly

148 increased the longitudinal VNC length in larvae and adult flies (Fig 2B,3C). In adults, the length
149 of the abdominal but not thoracic neuromeres of the VNC was elongated (Fig S5C). We then
150 sought to identify the glial cell type responsible for VNC elongation by enforcing *Bchs*
151 overexpression in glial subtypes through specific *Gal4* drivers. We found that *Bchs*
152 overexpression in subperineural glial cells (*rL82-Gal4*) was sufficient to increase the larval
153 VNC length, while overexpression in perineural (*c527-Gal4*) or wrapping glia (*nrv2-Gal4*) was
154 not (Fig S6). Subperineural glial cells are essential for the blood brain barrier (BBB) and form
155 septate junctions (Baumgartner *et al.* 1996; Stork *et al.* 2008). These data demonstrate that glial
156 *Bchs* plays a role in regulating CNS size.

157 Elongation of the VNC may be caused by an increased number of glial cells. Therefore,
158 we quantified the number of glial cells in the larval brain using an anti-repo antibody, which is
159 a panglial cell marker (Xiong *et al.* 1994). Panglial *Bchs* overexpression significantly increased
160 the number of repo^{+} nuclei but not their density (Fig 4A,B). We additionally observed an
161 increased number of glial cells in the peripheral nervous system (Fig S7). In conclusion, *Bchs*
162 overexpression can act on glial proliferation or apoptosis inside and outside the CNS.

163

164 ***Bchs overexpression causes protein accumulation and a shift towards non-acidic autophagic***
165 ***vesicles***

166 The autophagy adaptor ref(2)P links ubiquitinated proteins to autophagosomes via
167 interactions with Atg8a, which is anchored to autophagic compartment membranes (Jain *et al.*
168 2015). Aggregates of ref(2)P are considered as a marker of misfunctioning protein degradation
169 by autophagy or the ubiquitin-proteasome system (UPS) (Bartlett *et al.* 2011; Nezis *et al.* 2008;
170 Pircs *et al.* 2012). *Bchs* loss-of-function variants have been described to lead to a ref(2)P
171 (human homolog: p62) accumulation and an increase in early autophagic compartments,
172 suggesting an impaired autophagic flux (Clausen *et al.* 2010; Hebbar *et al.* 2015; Sim *et al.*

2019). To test whether *Bchs* overexpression impairs autophagy, ref(2)P immunostainings and an autophagic vesicle pH-reporter were utilized. Our data indicate strong accumulation of ref(2)P in the thoracic neuromeres of the VNC and milder also in the brain upon glial *Bchs* overexpression in the adult CNS (Fig 3A). Consistently, the overall larval CNS showed increased ref(2)P staining (Fig 2A).

In contrast, adult flies overexpressing *Bchs* panneuronally accumulated ref(2)P most prominently in the posterior region of the VNC but also with a lower signal intensity in the brain (Fig 3D). Larvae displayed ref(2)P aggregates in a subset of neurons in the VNC (Fig 2D), which we speculated to be motoneurons due to the flies' locomotion phenotype. Driving *Bchs* overexpression in motoneurons simultaneously with a membrane-bound GFP demonstrated that a subset of motoneurons did form ref(2)P aggregates in response to *Bchs* overexpression (Fig S4). It was previously shown that *Bchs* overexpression in *even-skipped* (eve)-positive motoneurons aCC and RP2 leads to morphological abnormalities and neuronal death (Lim und Kraut 2009; Hebbar et al. 2015; Sim et al. 2019). We thus hypothesized that the ref(2)P signal might localize to eve-positive neurons, and conducted a double immunostaining of eve and ref(2)P confirming that a small subset of eve-positive neurons accumulate ref(2)P (Fig S8). However, also eve-negative neurons showed ref(2)P expression.

We further applied a GFP-mCherry-Atg8a reporter to check the ratio of non-acidic to acidic autophagic vesicles in larval brains (Nezis *et al.* 2010). Fusion of an autophagosome with an endosome or lysosome results in an acidic autophagic vesicle, termed amphisome or autolysosome, respectively. GFP fluorescence is quenched in the acidic environment leading to an mCherry-only signal that does not colocalize with a concurrent GFP signal. In larvae overexpressing *Bchs* in glial cells, a significantly increased colocalization of mCherry and GFP signals was observed in comparison to the control indicating a shift of the ratio towards non-acidic autophagic vesicles (Fig 5A,B,C,S9A). Dissimilarly, in animals with panneuronal *Bchs*

198 overexpression no significant difference in the acidic environment of autophagic vesicles was
199 detected (Fig 5D,E,F,S9B). Collectively, the ref(2)P accumulation and change in autophagic
200 compartment acidity indicates that glial *Bchs* overexpression affects autophagic flux prior to or
201 at the step of acidification of autophagic vesicles.

202

203 ***Bchs overexpression leads to altered transcriptome profiles***

204 To understand which molecular pathways are affected by *Bchs* overexpression and how this
205 impacts brain function, we performed RNA-seq on heads from adult flies overexpressing *Bchs*
206 in glia or neurons. Although *Bchs* overexpression in glial cells caused a more severe phenotype
207 with differences in brain size and autophagy when compared to neuronal overexpression (Fig
208 3, 5), we identified more differentially expressed genes (i.e. genes with different expression in
209 *Bchs* overexpression flies as opposed to control animals carrying only the *Gal4* driver or only
210 the *UAS*-target gene) in the panneuronal *nSyb-Gal4/UAS-bchs::HA* condition (2,107 genes;
211 glial *Bchs* overexpression: 156 genes) (Tab S1). 79 genes were similarly differentially
212 expressed upon *Bchs* overexpression in glia and neurons, which represented a highly significant
213 overlap (p-value < 0.0001 from 1,000 simulations using 13,000 genes for random sampling).

214 Among the overlapping differentially expressed genes we identified *Iml1* and *Rab32* (Tab S1),
215 which are known to play an important role in autophagy (Hirota & Tanaka 2009; Wang *et al.*
216 2012; Wu & Tu 2011). The gene ontology (GO) categories enriched for both glial and neuronal
217 *Bchs* overexpression were related to extracellular space (Tab S1), hinting to the biological
218 provenance of the observed phenotypes. Additionally, for glial *Bchs* overexpression the GO
219 category septate junction (GO:0005918) was enriched. Whereas, neuronal *Bchs* overexpression
220 led to an enrichment of GO categories related to autophagy and mitochondria.

221 Taken together, there was a significant number of overlapping genes that suffered dysregulation
222 after *Bchs* overexpression in neurons or glial cells. This implies an altered molecular

mechanism regardless of the inquired cell type. We identified genes involved in autophagy and lysosome formation, but also an enrichment of genes annotated to the extracellular space.

Discussion

WDFY3 loss-of-function variants have been linked to neurodevelopmental and neurodegenerative disorders (Dragich *et al.* 2016; Finley *et al.* 2003; Le Duc *et al.* 2019; Orosco *et al.* 2014; Schaaf *et al.* 2022). Further, *WDFY3* variants have been associated with an increase or decrease in brain size (Finley *et al.* 2003; Kadir *et al.* 2016; Kriston-Vizi *et al.* 2011; Le Duc *et al.* 2019; Orosco *et al.* 2014). We hypothesized that variants underlying potential loss- or gain-of-function have opposing effects on brain size. Here, we used a *Drosophila Bchs* overexpression model as a proxy for gain-of-function effects in development. Ubiquitous *Bchs* overexpression was lethal (Fig S1), suggesting that *Bchs* expression levels are highly relevant also in non-neural tissue. We then overexpressed *Bchs* in different cell types of the nervous system to understand how dysregulation in different cells impacts development.

Bchs overexpression impaired nervous system, wing, and thorax development

We tested whether dysregulation of *WDFY3*/*Bchs* in glial cells may contribute to phenotypic abnormalities observed in probands with *WDFY3* variants. We detected a prolonged developmental time for flies overexpressing *Bchs* in glial cells, but not for panneuronal overexpression, indicating a role of glial *Bchs* in developmental processes (Fig 1A).

On the other side, neuronal *Bchs* overexpression caused higher rates of wing and thorax defects. Driving *Bchs* overexpression only in CCAP neurons was sufficient to cause these morphological phenotypes, implicating that CCAP neurons are responsible for wing and thorax abnormalities. CCAP neurons are well known to have a major role in post-ecdysis development

(Luan *et al.* 2006; Park *et al.* 2003). Suppressing their activity disrupts tonic abdominal contractions and air swallowing, a motor program necessary to pump hemolymph into wings to unfold them (Peabody *et al.* 2009). Further, CCAP neurons secrete the hormone bursicon, required for wing expansion and tanning, into the hemolymph (Dewey *et al.* 2004; Loveall & Deitcher 2010; Luo *et al.* 2005). Interestingly, similar wing and thorax abnormalities were noticed upon misexpression of *TBPH* (human ortholog: *TDP-43*), an RNA-binding protein, or knockdown of *Gclc*, an enzyme involved in glutathione synthesis, in CCAP neurons (Mercer *et al.* 2016; Vanden Broeck *et al.* 2013). Dysregulations of those genes were hypothesized to induce premature degeneration of CCAP neurons causing wing and thorax defects. Therefore, we suspect that also *Bchs* overexpression might have contributed to a degeneration of CCAP neurons. Importantly, WDFY3 is involved in the removal of mutant TDP-43 (Han *et al.* 2015), suggesting that *Bchs* overexpression might lead to a misregulation of TBPH in CCAP neurons. However, in our transcriptomic analyses, we did not identify *TBPH* or *Gclc* to be differentially expressed in flies overexpressing *Bchs* in neurons. On the other side, *Pburs*, a subunit of the hormone bursicon was upregulated (Tab S1, 10-fold higher expression, *adj-p*= 0.0008) (Luo *et al.* 2005). Null mutants of *Pburs* were similarly described to have a wing expansion deficit (Lahr *et al.* 2012). The observed weak penetrance of wing and thorax abnormalities in glial *Bchs* overexpression flies may indicate that in a small number of flies glial *Bchs* overexpression provoked a misfunctioning of CCAP neurons (Fig 1D,E). Similarly, the weak penetrance of abnormalities in motoneuronal *Bchs* overexpression could be explained by its expression in CCAP motoneurons but not in CCAP interneurons (Fig S3). Our data suggest that both, neuronal and glial *Bchs* dysregulation contribute to developmental defects. This is further supported by the impaired crawling behavior in glial and neuronal *Bchs* overexpression larvae (Fig 2C,F), which is in accordance with delayed motor development observed in affected patients (Le Duc *et al.* 2019).

Bchs affects CNS morphology

WDFY3 loss-of-function variants lead to an increased brain size in mice and humans (Le Duc *et al.* 2019; Orosco *et al.* 2014), while *Bchs* loss-of-function variants were described to reduce the brain size (Finley *et al.* 2003; Kriston-Vizi *et al.* 2011). Although dysregulated *WDFY3/Bchs* levels might have different downstream effects in the respective model organisms, we were still prompted to check whether the overexpression in the different nervous system cells impact the overall brain size.

In our study, only glial, but not neuronal, *Bchs* overexpression caused alterations in CNS size, presented in an elongated VNC and a decreased brain size to fly length ratio (Fig 2,3). In contrast, previous studies demonstrated that neuronal *Bchs* overexpression increases larval brain size (Kriston-Vizi *et al.* 2011). This discrepancy of neuronal overexpression phenotypes might be due to investigation of different developmental stages or because of using different neuronal drivers. Importantly, glial *Bchs* can influence the CNS size, demonstrating that glia need to be considered when examining the mechanism underlying altered CNS size. Furthermore, different cell types also of distinct stages of differentiation might contribute to the altered CNS size of *WDFY3*/*Bchs* mutants. The contribution of each cell type might depend on the observed developmental phase. In mice, Orosco *et al*. showed that hypomorphic variants of *Wdfy3* increase symmetric proliferation of radial glia, neural stem cells, which give rise to neurons and glia (Orosco *et al.* 2014). Interestingly, glial *Bchs* overexpression resulted in a gain of glial cell number (Fig 4,S7). This gain could have been caused similarly by increased proliferation of *Drosophila* neural stem cells (neuroblasts), intermediate progenitor cells or glial cells. It is well known that glial cells can regulate neuroblast proliferation (Contreras *et al.* 2021; Kanai *et al.* 2018; Nguyen & Cheng 2022; Yang *et al.* 2021). However, reduced glial cell death could also have provoked the cell number increase. Further studies are needed, to

297 determine whether the increased glial cell number is caused by alteration of proliferation or cell
298 death.

299 Several genes have been previously associated with elongated VNC as seen in glial *Bchs*
300 overexpression larvae (Fig 2), e.g. glial overexpression of the genes *mmp2* or *kuz,* encoding
301 metalloproteases (Dai *et al.* 2018; Kato *et al.* 2011; Losada-Perez *et al.* 2016; Meyer *et al.* 2014;
302 Pandey *et al.* 2011; Skeath *et al.* 2017; Winkler *et al.* 2021). Both proteases likely regulate BBB
303 integrity (Kanda *et al.* 2019; Petri *et al.* 2019). Subperineural glia form an essential part of the
304 BBB by producing septate junctions. Importantly, *Bchs* overexpression in subperineural glia
305 was sufficient to promote VNC elongation. Additionally, in our transcriptomic analyses we
306 found a dysregulation of genes associated with septate junctions (*Tsf2*, *kune*, *cold*, *gli*, *hoka*,
307 *udt*, Tab S1) in flies overexpressing *Bchs* in glial cells (Hijazi *et al.* 2011; Izumi *et al.* 2021;
308 Kanda *et al.* 2019; Nelson *et al.* 2010; Schulte *et al.* 2003; Tiklová *et al.* 2010). This suggests
309 that glial *Bchs* overexpression impairs proper septate junction formation and BBB integrity,
310 which could contribute to the altered brain size observed in different animal models and
311 probands.

312

313 ***Bchs overexpression impairs autophagic flux***

314 Further, transcriptomics analyses identified 2,107 and 156 genes to be differentially
315 expressed in flies overexpressing *Bchs* in neurons and glia, respectively (Tab S1). For neuronal
316 and glial *Bchs* overexpression, 50 and 3 of the differentially expressed genes, respectively, are
317 annotated to the GO category autophagy (GO:0006914) or its child terms. Those genes play
318 important roles in autophagy, which is the main known function of *WDFY3*/*Bchs*.

319 Bchs is an adaptor between ref(2)P and the autophagosomal membrane, therefore, a gain
320 of *Bchs* could be assumed to increase autophagic flux (Clausen *et al.* 2010; Filimonenko *et al.*
321 2010; Sim *et al.* 2019; Simonsen *et al.* 2004). However, our data showing ref(2)P aggregation

and a shifted ratio towards non-acidic autophagic vesicles when *Bchs* was overexpressed in glia suggest that the overexpression disrupts the autophagy pathway (Fig 2,3,5). Additionally, neuronal and glial *Bchs* overexpression decreased mRNA levels of the autophagy-associated genes *Iml1* and *Rab32* (*lightoid*) (Tab S1), further supporting a perturbed autophagic flux (Wang *et al.* 2012; Wu & Tu 2011). Nevertheless, we cannot rule out that formation of non-acidic autophagic vesicles was increased but the downstream autophagy pathway was limited by the fusion step, leading to an excessive build-up of non-acidic vesicles.

In both, larval and adult CNS, glial *Bchs* overexpression compared to neuronal *Bchs* overexpression resulted in a ref(2)P aggregation pattern that was more widely spread in the CNS (Fig 2,3). However, from ref(2)P accumulation it is not possible to conclude on the impact on neuronal function. Yet, recent research has shown that glial autophagy impacts neuronal health, e.g. in neurodegenerative diseases like Parkinson's disease and Alzheimer's disease (Bankston *et al.* 2019; Cho *et al.* 2014; Choi *et al.* 2020; Damulewicz *et al.* 2022; Kreher *et al.* 2021; Szabó *et al.* 2023; Tu *et al.* 2021).

In this study, we demonstrated that glial, as well as neuronal *Bchs* overexpression can lead to developmental abnormalities. While neurons have been implicated in *WDFY3*-associated pathologies, our data indicate that glial *Bchs* dysregulation also contributes to phenotypic defects. Since at least in respect to brain size *WDFY3*/*Bchs* was shown to yield different downstream effects in different model organisms, further investigations should be carried out to decipher the role of glial *WDFY3* in *WDFY3*-related neurodevelopmental disorders, and whether a modulation of glial function could rescue the phenotype.

Materials and Methods

Fly husbandry

Flies were maintained on standard cornmeal food at 25 °C and a 12:12 light-dark cycle. The following *Drosophila melanogaster* strains were used:

w^{1118}

;; repo-GAL4/TM6B Tb, (RRID:BDSC_7415)

;; nSyb-GAL4/Sb, (gift from J. Simpson)

; UAS-bchs::HA, (RRID:BDSC_51636)

;; act5C-Gal4/Tb,Sb, (RRID:BDSC_3954)

; ok6-GAL4 w^{+}, (Marqués *et al.* 2002)

; UASp-GFP-mCherry-Atg8a, (RRID:BDSC_37749)

; UAS-mCD8::GFP, UAS-mCD8::GFP, (RRID:BDSC_5137)

;; UAS-mCD8::GFP, (RRID:BDSC_5130)

; Burs-GAL4, (RRID:BDSC_40972)

;; CCAP-GAL4, (RRID:BDSC_25686)

; rL82-GAL4, (Sepp & Auld 1999)

; nrv2-GAL4, (RRID:BDSC_6800)

;; c527-Gal4, (RRID:BDSC_90391)

Mendelian ratio and adult developmental time

15 virgin females (*UAS-bchs::HA/*Sb^1) and 5 males (cell type-specific reporter-*Gal4/*Sb^1), all carrying the balancer chromosome (marker: Sb^1), were crossed and switched to a new vial every day. Numbers of flies carrying the balancer chromosome (no *Bchs* overexpression) and flies not carrying the balancer (*Bchs* overexpression) in the F1 generation

368 of five vials were counted for each genotype. Newly hatched flies were counted every 24 h. For
369 each vial, counting was started on the day the first adult fly hatched and continued for ten days.

370

371 ***PEDtracker – embryonal developmental time, larval and pupal size***

372 The development of panneuronal *Bchs* overexpression flies (*nSyb-Gal4/UAS-bchs::HA*)
373 as well as the controls *nSyb-Gal4/+* and *UAS-bchs::HA/+* was monitored using the PEDtracker
374 system (Schumann & Triphan 2020). According to the previously published protocol, the
375 development of the specimen was observed from egg hatching to pupation. Larval hatching
376 timepoint, larval size over development as well as pupal size were then manually measured
377 using ImageJ (Schneider *et al.* 2012). Statistical analysis was performed using Kruskal-Wallis
378 test or one-way ANOVA depending on the distribution of the data.

379

380 ***Assessing the condition of wings and thoraces***

381 20 virgin females and 10 males were crossed and switched to a new vial every second
382 day. For each genotype, the F1 generation in three vials was analysed. For each vial, collecting
383 flies was started on the day the first adult fly hatched and continued for five days. The condition
384 of wings and thoraces was evaluated 24 h after collecting the flies (24−48 h old flies). Wings
385 were categorized into folded, partially folded, and expanded. Thoraces were categorized into
386 dimpled and not dimpled.

387

388 ***Larval locomotion***

389 Petri dishes with a diameter of 9 cm filled with 1 % agarose were prepared. Five third
390 instar larvae were placed in the middle of a petri dish and recorded (camera: Logitech C920
391 HD Pro) for 1 min. The first 5 sec of a recording were dismissed and larval behavior of the

following 30 sec investigated. Recordings were analysed by using the ImageJ freehand line tool to measure the length of the crawled route of a larva. For each genotype, 30 larvae were examined if not stated otherwise.

Immunohistochemistry

Larvae: Wandering third instar larvae were dissected in ice-cold HL-3 solution (Stewart *et al.* 1994), fixed with PFA (4 % in PBS) and collected in 1× PBS. Blocking, primary antibody incubation and secondary antibody incubation were consecutively performed in PBT (1× PBS + 0.05 % Triton X-100, Sigma-Aldrich) containing 5 % normal goat serum (NGS, Jackson ImmunoResearch) at 4°C overnight. Antibody incubation steps were followed by washing two times shortly and three times 15 min (1× PBS + 0.05 % Triton X-100). Samples were stored in Vectashield (Vector Laboratories) at 4°C overnight before mounting.

Adult flies: The CNS of adult female flies (21−33 h old) were dissected in ice-cold Ringer solution, fixed in 4 % PFA for 30 min at room temperature and collected in 1× PBS. Blocking was done at room temperature for 24 h in PBT (1× PBS + 1 % Triton X-100) containing 5 % NGS. Primary antibody incubation was carried out at 4°C for 24 h and secondary antibody incubation at 4°C for 24−48 h. Antibody incubation steps were followed by moving samples to room temperature for 1 h and washing two times shortly and three times 15 min with PBT. Samples were stored in Vectashield at 4°C overnight before mounting.

The following antibodies were used at following dilutions: rabbit-anti-Ref(2)P (1:500, Abcam, ab178440), mouse-anti-repo (1:250, DSHB, 8D12 concentrate), mouse-anti-even skipped (1:50, DSHB, 2B8), goat-anti-mouse conjugated with Alexa Fluor-488 or -405 (1:250, Invitrogen, A-11001, RRID: AB_2534069 and A-31553, RRID: AB_221604), goat-anti-horseradish peroxidase (HRP) conjugated with Alexa Fluor-488 or -647 (1:250, Jackson ImmunoResearch, 123-545-021, RRID: AB_2338965 and 123-605-021, RRID: AB_2338967),

Cy3- or Cy5-conjugated goat-anti-rabbit (1:250, Jackson ImmunoResearch, 111-165-144, RRID:AB_2338006 and 111-175-144, RRID: AB_2338013).

Central nervous system size measurement

Larval VNC was measured and normalized to the larval length which was determined before dissection. Larvae were placed into a petri dish filled with HL-3 on ice and imaged (camera: Leica DFC365 FX, microscope: Leica MZ10 F). Brains were stained against HRP, imaged and a maximum projection of the z-stack was performed with ImageJ. The length of the larvae and the VNC were measured with the ImageJ Straight Line tool.

The size of the VNC and the brain of adult flies was determined and normalized to the fly length. The adult fly was anesthetized by putting it in a vial on ice. The fly was transferred to a petri dish and imaged (camera: Leica DFC365 FX, microscope: Leica MZ10 F). The central nervous system was stained against HRP, imaged, and a maximum projection was performed. Lengths of the fly and the VNC were measured with the ImageJ Straight Line tool. The area of the brain was measured with the ImageJ Freehand selection tool.

Number of glial cells

Larvae were stained with anti-repo antibody and imaged. Repo-positive nuclei were counted using the ImageJ plugin cell counter. For analysis of glial cell number in the peripheral nervous system, glial nuclei number was determined at the entry point of the peripheral nerve bundle into the body wall muscles at the region, where the bundle divides into the TN, ISN, and SN nerve branches. Peripheral nerves innervating the hemisegments A4R and A4L were analysed.

Colocalization of GFP-mCherry-Atg8 fluorophore signals

Larval brains were dissected and fixed as described before, stored in Vectashield for at least 24 h and imaged. Images were deconvoluted using Huygens Essentials software (strategy: standard). Analyses of images were performed with the ImageJ plugin coloc 2 (Pearson correlation, above threshold) and using the freehand selection tool to set a ROI surrounding the brain.

Imaging

Image acquisition was performed with a Leica SP8 confocal microscope unless specified otherwise.

RNA extraction and sequencing

RNA was extracted from five female and five male fly heads for one sample. Flies (22−31 h after eclosion) were anesthetized with carbon dioxide and heads were cut using a scalpel. Heads were immediately transferred to an ice-cold 2 ml Eppendorf tube containing Trizol or RLT buffer. RNA extraction followed immediately using the RNeasy Micro Kit (Qiagen, Cat. No. 74004) according to protocol or exchanging the first step of homogenization in RLT buffer with the following Trizol protocol (Invitrogen, Cat. No. 15596026). Heads were homogenized in 500 µl Trizol, centrifuged for 5 min at 10,000 rpm at 4°C, supernatant was tranferred to a new tube, 200 µl chloroform (Carl Roth, No. 6340.1) was added and the tube was shaken for 15 sec. An incubation step at room temperature for 3 min was followed by centrifugation for 5 min at 10,000 rpm at 4°C. The upper aqueous phase was transferred in a new tube and it was continued with the RNeasy Micro Kit protocol. Homogenization was

464 performed on ice using the Ultra-Turrax (IKA T10 basic) five times for 10 sec. For each
465 genotype five samples were sequenced.

466 RNA-seq libraries were prepared using TruSeq RNA Library Prep Kit v2 (Illumina, San
467 Diego, CA) and sequenced on an Illumina NovaSeq platform with 151 bp paired-end reads with
468 an average of ~135 million reads per library.

469

470 ***Differential Gene Expression (DEG) analysis***

471 RNA-Seq reads were mapped to the Drosophila genome assembly BDGP6.32
472 (GCA_000001215.4) with STAR (version 2.6.1d) (Dobin *et al.* 2013). Reads were processed
473 as previously described (Körner *et al.* 2022). We computed the transcript levels with htseq-
474 count (version 0.6.0) (Anders *et al.* 2015). Genes with a sum of less than 10 reads in all samples
475 together were excluded from further analysis. Differential expression of genes was determined
476 with the R package DESeq2 (version 1.30.1) (Love *et al.* 2014), which uses the Benjamini-
477 Hochberg method to correct for multiple testing (Benjamini *et al.* 2001). Genes were considered
478 to be significantly differentially expressed if p-adj < 0.05. To check clustering of RNA-
479 sequencing samples of subjects and controls, a principal component analysis (PCA) was
480 performed with the R package pcaExplorer (version 2.6.0) (Marini und Binder 2019). RNA
481 count data were variance stabilized transformed and the 500 most variable genes (top n genes)
482 were selected for computing the principal components. We tested 5 samples of adult heads from
483 glial/neuronal *Bchs* overexpression (*repo-Gal4/UAS-bchs::HA* and *nSyb-Gal4/UAS-bchs::HA*,
484 respectively) against the pooled samples of both controls, 5 samples of the *Gal4*-driver control
485 (*repo-Gal4/+* and *nSyb-Gal4/+*, respectively) and 5 samples of the *UAS* control (*UAS-*
486 *bchs::HA/+*).

To identify which pathways are enriched with differentially expressed genes we used the GOfuncR package with a hypergeometric test and the Drosophila GO annotations org.Dm.eg.db v.3.17 (Carlson 2019; Grote 2021).

Statistics

Data are shown as mean ± SEM. Statistical analyses were performed with SigmaPlot 12.5 (Systat software) using two-tailed Student's t-tests or Mann-Whitney Rank Sum test for non-normally distributed data, if not stated otherwise.

Competing interest statement

The authors declare no competing interests.

Acknowledgments

We thank Anne Butthof for advices on RNA extraction protocol, Mathias Böhme for discussion about glial cells and Torsten Schöneberg for useful discussions which led to new insights in respect to the pathomechanism.

Author contributions

MK performed fly experiments, contributed to the experimental design and wrote the first draft of the manuscript. AV and LB performed gene expression and GO enrichment analyses. IS and JK performed PEDtracker assays and contributed to writing of the manuscript. KK, KD and JH performed RNA and DNA sequencing. AG, AT and RAJ contributed to result interpretation and writing of the manuscript. NS, AM and TL contributed to design of the study, data

510 interpretation, funding acquisition, and writing of the manuscript. DLD designed and
511 supervised the study, acquired funding, and contributed to writing of the manuscript.

512

513 **Funding**

514 This work was supported by the Else Kröner-Fresenius-Stiftung 2020_EKEA.42 to DLD and
515 the German Research Foundation SFB 1052 project B10 to DLD and AG. DLD and AM are
516 fellows of the Clinician Scientist program of the Leipzig University Medical Center. AM
517 received funding from Jung Foundation for Science and Research through Jung Career
518 Advancement Prize 2023. NS and TL were funded by the German Research Foundation through
519 CRC 1423, project B06 (project number 421152132). NS was supported through a Junior
520 research grant from the Faculty of Medicine, Leipzig University. AT was supported by the
521 German Research Foundation (Grant No. 441181781, 426722269, 432195391) and by EU
522 funds from the ESF Plus Program (Grant No. 100649752). Mutant and transgenic fly stocks
523 were obtained from the Bloomington Drosophila Stock Center (NIH P40OD018537).

524

525 **Availability of data and materials**

526 RNA-seq data has been submitted to the Gene Expression Omnibus
527 (http://www.ncbi.nlm.nih.gov/geo/) under accession number GSE244775.

528

529 **References**

530 Aber ER, Griffey CJ, Davies T, Li AM, Yang YJ, Croce KR, Goldman JE, Grutzendler J,
531 Canman JC & Yamamoto A (2022). Oligodendroglial macroautophagy is essential for
532 myelin sheath turnover to prevent neurodegeneration and death, *Cell Rep* **41**, 111480;
533 DOI: 10.1016/j.celrep.2022.111480.

534 Anders S, Pyl PT & Huber W (2015). HTSeq—a Python framework to work with high-
535 throughput sequencing data, *Bioinformatics* **31**, 166–169; DOI:
536 10.1093/bioinformatics/btu638.

537 Bankston AN, Forston MD, Howard RM, Andres KR, Smith AE, Ohri SS, Bates ML, Bunge
538 MB & Whittemore SR (2019). Autophagy is essential for oligodendrocyte differentiation,
539 survival, and proper myelination, *Glia* **67**, 1745–1759; DOI: 10.1002/glia.23646.

540 Bartlett BJ, Isakson P, Lewerenz J, Sanchez H, Kotzebue RW, Cumming RC, Harris GL,
541 Nezis IP, Schubert DR & Simonsen A, et al. (2011). p62, Ref(2)P and ubiquitinated
542 proteins are conserved markers of neuronal aging, aggregate formation and progressive
543 autophagic defects, *Autophagy* **7**, 572–583; DOI: 10.4161/auto.7.6.14943.

544 Baumgartner S, Littleton JT, Broadie K, Bhat MA, Harbecke R, Lengyel JA, Chiquet-
545 Ehrismann R, Prokop A & Bellen HJ (1996). A Drosophila neurexin is required for septate
546 junction and blood-nerve barrier formation and function, *Cell* **87**, 1059–1068; DOI:
547 10.1016/s0092-8674(00)81800-0.

548 Benjamini Y, Drai D, Elmer G, Kafkafi N & Golani I (2001). Controlling the false discovery
549 rate in behavior genetics research, *Behav Brain Res* **125**, 279–284; DOI: 10.1016/s0166-
550 4328(01)00297-2.

551 Bittern J, Pogodalla N, Ohm H, Brüser L, Kottmeier R, Schirmeier S & Klämbt C (2021).
552 Neuron-glia interaction in the Drosophila nervous system, *Dev Neurobiol* **81**, 438–452;
553 DOI: 10.1002/dneu.22737.

554 Carlson M (2019). *org.Dm.eg.db: Genome wide annotation for Fly. R package version 3.8.2*.

555 Cho M-H, Cho K, Kang H-J, Jeon E-Y, Kim H-S, Kwon H-J, Kim H-M, Kim D-H & Yoon
556 S-Y (2014). Autophagy in microglia degrades extracellular β-amyloid fibrils and regulates
557 the NLRP3 inflammasome, *Autophagy* **10**, 1761–1775; DOI: 10.4161/auto.29647.

558 Choi I, Zhang Y, Seegobin SP, Pruvost M, Wang Q, Purtell K, Zhang B & Yue Z (2020).
559 Microglia clear neuron-released α-synuclein via selective autophagy and prevent
560 neurodegeneration, *Nat Commun* **11**, 1386; DOI: 10.1038/s41467-020-15119-w.

561 Clausen TH, Lamark T, Isakson P, Finley K, Larsen KB, Brech A, Øvervatn A, Stenmark H,
562 Bjørkøy G & Simonsen A, et al. (2010). p62/SQSTM1 and ALFY interact to facilitate the
563 formation of p62 bodies/ALIS and their degradation by autophagy, *Autophagy* **6**, 330–344;
564 DOI: 10.4161/auto.6.3.11226.

565 Contreras EG, Glavic Á, Brand AH & Sierralta JA (2021). The Serine Protease Homolog,
566 Scarface, Is Sensitive to Nutrient Availability and Modulates the Development of the
567 Drosophila Blood-Brain Barrier, *J. Neurosci.* **41**, 6430–6448; DOI:
568 10.1523/JNEUROSCI.0452-20.2021.

569 Dai J, Estrada B, Jacobs S, Sánchez-Sánchez BJ, Tang J, Ma M, Magadán-Corpas P, Pastor-
570 Pareja JC & Martín-Bermudo MD (2018). Dissection of Nidogen function in Drosophila
571 reveals tissue-specific mechanisms of basement membrane assembly, *PLoS Genet* **14**,
572 e1007483; DOI: 10.1371/journal.pgen.1007483.

573 Damulewicz M, Szypulski K & Pyza E (2022). Glia-Neurons Cross-Talk Regulated Through
574 Autophagy, *Front Physiol* **13**, 886273; DOI: 10.3389/fphys.2022.886273.

575 Dewey EM, McNabb SL, Ewer J, Kuo GR, Takanishi CL, Truman JW & Honegger H-W
576 (2004). Identification of the gene encoding bursicon, an insect neuropeptide responsible for
577 cuticle sclerotization and wing spreading, *Curr Biol* **14**, 1208–1213; DOI:
578 10.1016/j.cub.2004.06.051.

579 DiAntonio A, Burgess RW, Chin AC, Deitcher DL, Scheller RH & Schwarz TL (1993).
580 Identification and characterization of Drosophila genes for synaptic vesicle proteins, *J.*
581 *Neurosci.* **13**, 4924–4935; DOI: 10.1523/JNEUROSCI.13-11-04924.1993.

582 Dobin A, Davis CA, Schlesinger F, Drenkow J, Zaleski C, Jha S, Batut P, Chaisson M &
583 Gingeras TR (2013). STAR: ultrafast universal RNA-seq aligner, *Bioinformatics* **29**, 15–
584 21; DOI: 10.1093/bioinformatics/bts635.

585 Dragich JM, Kuwajima T, Hirose-Ikeda M, Yoon MS, Eenjes E, Bosco JR, Fox LM, Lystad
586 AH, Oo TF & Yarygina O, et al. (2016). Autophagy linked FYVE (Alfy/WDFY3) is
587 required for establishing neuronal connectivity in the mammalian brain, *eLife* **5**; DOI:
588 10.7554/eLife.14810.

589 Filimonenko M, Isakson P, Finley KD, Anderson M, Jeong H, Melia TJ, Bartlett BJ, Myers
590 KM, Birkeland HCG & Lamark T, et al. (2010). The selective macroautophagic
591 degradation of aggregated proteins requires the PI3P-binding protein Alfy, *Mol Cell* **38**,
592 265–279; DOI: 10.1016/j.molcel.2010.04.007.

593 Finley KD, Edeen PT, Cumming RC, Mardahl-Dumesnil MD, Taylor BJ, Rodriguez MH,
594 Hwang CE, Benedetti M & McKeown M (2003). blue cheese Mutations Define a Novel,
595 Conserved Gene Involved in Progressive Neural Degeneration, *J. Neurosci.* **23**, 1254–
596 1264; DOI: 10.1523/JNEUROSCI.23-04-01254.2003.

597 Fox LM, Kim K, Johnson CW, Chen S, Croce KR, Victor MB, Eenjes E, Bosco JR, Randolph
598 LK & Dragatsis I, et al. (2020). Huntington's Disease Pathogenesis Is Modified In Vivo by
599 Alfy/Wdfy3 and Selective Macroautophagy, *Neuron* **105**, 813-821.e6; DOI:
600 10.1016/j.neuron.2019.12.003.

601 Grote S (2021). *GOfuncR: Gene ontology enrichment using FUNC. R package version 1.14.0.*

602 Han H, Wei W, Duan W, Guo Y, Li Y, Wang J, Bi Y & Li C (2015). Autophagy-linked
603 FYVE protein (Alfy) promotes autophagic removal of misfolded proteins involved in
604 amyotrophic lateral sclerosis (ALS), *In Vitro Cell Dev Biol Anim* **51**, 249–263; DOI:
605 10.1007/s11626-014-9832-4.

606 Hebbar S, Sahoo I, Matysik A, Argudo Garcia I, Osborne KA, Papan C, Torta F,
607 Narayanaswamy P, Fun XH & Wenk MR, et al. (2015). Ceramides And Stress Signalling
608 Intersect With Autophagic Defects In Neurodegenerative Drosophila blue cheese (bchs)
609 Mutants, *Sci Rep* **5**, 15926; DOI: 10.1038/srep15926.

610 Hijazi A, Haenlin M, Waltzer L & Roch F (2011). The Ly6 protein coiled is required for
611 septate junction and blood brain barrier organisation in Drosophila, *PLoS ONE* **6**, e17763;
612 DOI: 10.1371/journal.pone.0017763.

613 Hirota Y & Tanaka Y (2009). A small GTPase, human Rab32, is required for the formation of
614 autophagic vacuoles under basal conditions, *Cell Mol Life Sci* **66**, 2913–2932; DOI:
615 10.1007/s00018-009-0080-9.

616 Izumi Y, Furuse K & Furuse M (2021). The novel membrane protein Hoka regulates septate
617 junction organization and stem cell homeostasis in the Drosophila gut, *J Cell Sci* **134**; DOI:
618 10.1242/jcs.257022.

619 Jain A, Rusten TE, Katheder N, Elvenes J, Bruun J-A, Sjøttem E, Lamark T & Johansen T
620 (2015). p62/Sequestosome-1, Autophagy-related Gene 8, and Autophagy in Drosophila
621 Are Regulated by Nuclear Factor Erythroid 2-related Factor 2 (NRF2), Independent of
622 Transcription Factor TFEB, *J Biol Chem* **290**, 14945–14962; DOI:
623 10.1074/jbc.M115.656116.

624 Kadir R, Harel T, Markus B, Perez Y, Bakhrat A, Cohen I, Volodarsky M, Feintsein-Linial
625 M, Chervinski E & Zlotogora J, et al. (2016). ALFY-Controlled DVL3 Autophagy
626 Regulates Wnt Signaling, Determining Human Brain Size, *PLoS Genet* **12**, e1005919;
627 DOI: 10.1371/journal.pgen.1005919.

628 Kanai MI, Kim M-J, Akiyama T, Takemura M, Wharton K, O'Connor MB & Nakato H
629 (2018). Regulation of neuroblast proliferation by surface glia in the Drosophila larval
630 brain, *Sci Rep* **8**, 3730; DOI: 10.1038/s41598-018-22028-y.

631 Kanda H, Shimamura R, Koizumi-Kitajima M & Okano H (2019). Degradation of
632 Extracellular Matrix by Matrix Metalloproteinase 2 Is Essential for the Establishment of
633 the Blood-Brain Barrier in Drosophila, *iScience* **16**, 218–229; DOI:
634 10.1016/j.isci.2019.05.027.

635 Karlsson M, Zhang C, Méar L, Zhong W, Digre A, Katona B, Sjöstedt E, Butler L, Odeberg J
636 & Dusart P, et al. (2021). A single-cell type transcriptomics map of human tissues, *Sci Adv*
637 **7**; DOI: 10.1126/sciadv.abh2169.

638 Kato K, Forero MG, Fenton JC & Hidalgo A (2011). The glial regenerative response to
639 central nervous system injury is enabled by pros-notch and pros-NFκB feedback, *PLoS*
640 *Biol* **9**, e1001133; DOI: 10.1371/journal.pbio.1001133.

641 Khodosh R, Augsburger A, Schwarz TL & Garrity PA (2006). Bchs, a BEACH domain
642 protein, antagonizes Rab11 in synapse morphogenesis and other developmental events,
643 *Development* **133**, 4655–4665; DOI: 10.1242/dev.02650.

644 Kim YS, Choi J & Yoon B-E (2020). Neuron-Glia Interactions in Neurodevelopmental
645 Disorders, *Cells* **9**; DOI: 10.3390/cells9102176.

646 Körner MB, Velluva A, Bundalian L, Radtke M, Lin C-C, Zacher P, Bartolomaeus T, Kirstein
647 AS, Mrestani A & Scholz N, et al. (2022). Altered gene expression profiles impair the
648 nervous system development in individuals with 15q13.3 microdeletion, *Sci Rep* **12**,
649 13507; DOI: 10.1038/s41598-022-17604-2.

650 Kraut R, Menon K & Zinn K (2001). A gain-of-function screen for genes controlling motor
651 axon guidance and synaptogenesis in Drosophila, *Curr Biol* **11**, 417–430; DOI:
652 10.1016/S0960-9822(01)00124-5.

653 Kreher C, Favret J, Maulik M & Shin D (2021). Lysosomal Functions in Glia Associated with
654 Neurodegeneration, *Biomolecules* **11**; DOI: 10.3390/biom11030400.

655 Kriston-Vizi J, Thong NW, Poh CL, Yee KC, Ling JSP, Kraut R & Wasser M (2011). Gebiss:
656 an ImageJ plugin for the specification of ground truth and the performance evaluation of
657 3D segmentation algorithms, *BMC Bioinformatics* **12**, 232; DOI: 10.1186/1471-2105-12-
658 232.

659 Lago-Baldaia I, Fernandes VM & Ackerman SD (2020). More Than Mortar: Glia as
660 Architects of Nervous System Development and Disease, *Front Cell Dev Biol* **8**, 611269;
661 DOI: 10.3389/fcell.2020.611269.

662 Lahr EC, Dean D & Ewer J (2012). Genetic analysis of ecdysis behavior in Drosophila
663 reveals partially overlapping functions of two unrelated neuropeptides, *J. Neurosci.* **32**,
664 6819–6829; DOI: 10.1523/JNEUROSCI.5301-11.2012.

665 Le Duc D, Giulivi C, Hiatt SM, Napoli E, Panoutsopoulos A, Harlan De Crescenzo A,
666 Kotzaeridou U, Syrbe S, Anagnostou E & Azage M, et al. (2019). Pathogenic WDFY3
667 variants cause neurodevelopmental disorders and opposing effects on brain size, *Brain*
668 **142**, 2617–2630; DOI: 10.1093/brain/awz198.

669 Lim A & Kraut R (2009). The Drosophila BEACH family protein, blue cheese, links
670 lysosomal axon transport with motor neuron degeneration, *J. Neurosci.* **29**, 951–963; DOI:
671 10.1523/JNEUROSCI.2582-08.2009.

672 Losada-Perez M, Harrison N & Hidalgo A (2016). Molecular mechanism of central nervous
673 system repair by the Drosophila NG2 homologue kon-tiki, *J Cell Biol* **214**, 587–601; DOI:
674 10.1083/jcb.201603054.

675 Love MI, Huber W & Anders S (2014). Moderated estimation of fold change and dispersion
676 for RNA-seq data with DESeq2, *Genome Biol* **15**, 550; DOI: 10.1186/s13059-014-0550-8.

677 Loveall BJ & Deitcher DL (2010). The essential role of bursicon during Drosophila
678 development, *BMC Dev Biol* **10**, 92; DOI: 10.1186/1471-213X-10-92.

679 Luan H, Lemon WC, Peabody NC, Pohl JB, Zelensky PK, Wang D, Nitabach MN, Holmes
680 TC & White BH (2006). Functional dissection of a neuronal network required for cuticle
681 tanning and wing expansion in Drosophila, *J. Neurosci.* **26**, 573–584; DOI:
682 10.1523/JNEUROSCI.3916-05.2006.

683 Luo C-W, Dewey EM, Sudo S, Ewer J, Hsu SY, Honegger H-W & Hsueh AJW (2005).
684 Bursicon, the insect cuticle-hardening hormone, is a heterodimeric cystine knot protein that
685 activates G protein-coupled receptor LGR2, *Proc Natl Acad Sci U S A* **102**, 2820–2825;
686 DOI: 10.1073/pnas.0409916102.

687 Marqués G, Bao H, Haerry TE, Shimell MJ, Duchek P, Zhang B & O'Connor MB (2002).
688 The Drosophila BMP type II receptor Wishful Thinking regulates neuromuscular synapse
689 morphology and function, *Neuron* **33**, 529–543; DOI: 10.1016/s0896-6273(02)00595-0.

690 Mercer SW, La Fontaine S, Warr CG & Burke R (2016). Reduced glutathione biosynthesis in
691 Drosophila melanogaster causes neuronal defects linked to copper deficiency, *J*
692 *Neurochem* **137**, 360–370; DOI: 10.1111/jnc.13567.

693 Meyer S, Schmidt I & Klämbt C (2014). Glia ECM interactions are required to shape the
694 Drosophila nervous system, *Mech Dev* **133**, 105–116; DOI: 10.1016/j.mod.2014.05.003.

695 Nelson KS, Furuse M & Beitel GJ (2010). The Drosophila Claudin Kune-kune is required for
696 septate junction organization and tracheal tube size control, *Genetics* **185**, 831–839; DOI:
697 10.1534/genetics.110.114959.

698 Nezis IP, Shravage BV, Sagona AP, Lamark T, Bjørkøy G, Johansen T, Rusten TE, Brech A,
699 Baehrecke EH & Stenmark H (2010). Autophagic degradation of dBruce controls DNA
700 fragmentation in nurse cells during late Drosophila melanogaster oogenesis, *J Cell Biol*
701 **190**, 523–531; DOI: 10.1083/jcb.201002035.

702 Nezis IP, Simonsen A, Sagona AP, Finley K, Gaumer S, Contamine D, Rusten TE, Stenmark
703 H & Brech A (2008). Ref(2)P, the Drosophila melanogaster homologue of mammalian
704 p62, is required for the formation of protein aggregates in adult brain, *J Cell Biol* **180**,
705 1065–1071; DOI: 10.1083/jcb.200711108.

706 Nguyen P-K & Cheng LY (2022). Non-autonomous regulation of neurogenesis by extrinsic
707 cues: a Drosophila perspective, *Oxf Open Neurosci* **1**; DOI: 10.1093/oons/kvac004.

708 Orosco LA, Ross AP, Cates SL, Scott SE, Wu D, Sohn J, Pleasure D, Pleasure SJ,
709 Adamopoulos IE & Zarbalis KS (2014). Loss of Wdfy3 in mice alters cerebral cortical
710 neurogenesis reflecting aspects of the autism pathology, *Nat Commun* **5**, 4692; DOI:
711 10.1038/ncomms5692.

712 Pandey R, Blanco J & Udolph G (2011). The glucuronyltransferase GlcAT-P is required for
713 stretch growth of peripheral nerves in Drosophila, *PLoS ONE* **6**, e28106; DOI:
714 10.1371/journal.pone.0028106.

715 Park JH, Schroeder AJ, Helfrich-Förster C, Jackson FR & Ewer J (2003). Targeted ablation of
716 CCAP neuropeptide-containing neurons of Drosophila causes specific defects in execution
717 and circadian timing of ecdysis behavior, *Development* **130**, 2645–2656; DOI:
718 10.1242/dev.00503.

719 Peabody NC, Pohl JB, Diao F, Vreede AP, Sandstrom DJ, Wang H, Zelensky PK & White
720 BH (2009). Characterization of the decision network for wing expansion in Drosophila
721 using targeted expression of the TRPM8 channel, *J. Neurosci.* **29**, 3343–3353; DOI:
722 10.1523/JNEUROSCI.4241-08.2009.

723 Petri J, Syed MH, Rey S & Klämbt C (2019). Non-Cell-Autonomous Function of the GPI-
724 Anchored Protein Undicht during Septate Junction Assembly, *Cell Rep* **26**, 1641-1653.e4;
725 DOI: 10.1016/j.celrep.2019.01.046.

726 Pircs K, Nagy P, Varga A, Venkei Z, Erdi B, Hegedus K & Juhasz G (2012). Advantages and
727 limitations of different p62-based assays for estimating autophagic activity in Drosophila,
728 *PLoS ONE* **7**, e44214; DOI: 10.1371/journal.pone.0044214.

729 Rahman MM, Islam MR, Yamin M, Islam MM, Sarker MT, Meem AFK, Akter A, Emran
730 TB, Cavalu S & Sharma R (2022). Emerging Role of Neuron-Glia in Neurological
731 Disorders: At a Glance, *Oxid Med Cell Longev* **2022**, 3201644; DOI:
732 10.1155/2022/3201644.

733 Schaaf ZA, Tat L, Cannizzaro N, Green R, Rülicke T, Hippenmeyer S & Zarbalis KS (2022).
734 WDFY3 mutation alters laminar position and morphology of cortical neurons, *Mol Autism*
735 **13**, 27; DOI: 10.1186/s13229-022-00508-3.

736 Schneider CA, Rasband WS & Eliceiri KW (2012). NIH Image to ImageJ: 25 years of image
737 analysis, *Nat Methods* **9**, 671–675; DOI: 10.1038/nmeth.2089.

738 Schulte J, Tepass U & Auld VJ (2003). Gliotactin, a novel marker of tricellular junctions, is
739 necessary for septate junction development in Drosophila, *J Cell Biol* **161**, 991–1000;
740 DOI: 10.1083/jcb.200303192.

741 Schumann I & Triphan T (2020). The PEDtracker: An Automatic Staging Approach for
742 Drosophila melanogaster Larvae, *Front. Behav. Neurosci.* **14**, 612313; DOI:
743 10.3389/fnbeh.2020.612313.

744 Sepp KJ & Auld VJ (1999). Conversion of lacZ enhancer trap lines to GAL4 lines using
745 targeted transposition in Drosophila melanogaster, *Genetics* **151**, 1093–1101; DOI:
746 10.1093/genetics/151.3.1093.

747 Sepp KJ, Schulte J & Auld VJ (2001). Peripheral glia direct axon guidance across the
748 CNS/PNS transition zone, *Dev Biol* **238**, 47–63; DOI: 10.1006/dbio.2001.0411.

749 Sim J, Osborne KA, Argudo García I, Matysik AS & Kraut R (2019). The BEACH Domain Is
750 Critical for Blue Cheese Function in a Spatial and Epistatic Autophagy Hierarchy, *Front*
751 *Cell Dev Biol* **7**, 129; DOI: 10.3389/fcell.2019.00129.

752 Simonsen A, Birkeland HCG, Gillooly DJ, Mizushima N, Kuma A, Yoshimori T, Slagsvold
753 T, Brech A & Stenmark H (2004). Alfy, a novel FYVE-domain-containing protein
754 associated with protein granules and autophagic membranes, *J Cell Sci* **117**, 4239–4251;
755 DOI: 10.1242/jcs.01287.

756 Skeath JB, Wilson BA, Romero SE, Snee MJ, Zhu Y & Lacin H (2017). The extracellular
757 metalloprotease AdamTS-A anchors neural lineages in place within and preserves the
758 architecture of the central nervous system, *Development* **144**, 3102–3113; DOI:
759 10.1242/dev.145854.

760 Søreng K, Pankiv S, Bergsmark C, Haugsten EM, Dahl AK, La Ballina LR de, Yamamoto A,
761 Lystad AH & Simonsen A (2022). ALFY localizes to early endosomes and cellular
762 protrusions to facilitate directional cell migration, *J Cell Sci* **135**; DOI:
763 10.1242/jcs.259138.

764 Stessman HAF, Xiong B, Coe BP, Wang T, Hoekzema K, Fenckova M, Kvarnung M, Gerdts
765 J, Trinh S & Cosemans N, et al. (2017). Targeted sequencing identifies 91
766 neurodevelopmental-disorder risk genes with autism and developmental-disability biases,
767 *Nat Genet* **49**, 515–526; DOI: 10.1038/ng.3792.

768 Stewart BA, Atwood HL, Renger JJ, Wang J & Wu CF (1994). Improved stability of
769 Drosophila larval neuromuscular preparations in haemolymph-like physiological solutions,
770 *J Comp Physiol A* **175**, 179–191; DOI: 10.1007/BF00215114.

771 Stork T, Engelen D, Krudewig A, Silies M, Bainton RJ & Klämbt C (2008). Organization and
772 function of the blood-brain barrier in Drosophila, *J. Neurosci.* **28**, 587–597; DOI:
773 10.1523/JNEUROSCI.4367-07.2008.

774 Szabó Á, Vincze V, Chhatre AS, Jipa A, Bognár S, Varga KE, Banik P, Harmatos-Ürmösi A,
775 Neukomm LJ & Juhász G (2023). LC3-associated phagocytosis promotes glial degradation
776 of axon debris after injury in Drosophila models, *Nat Commun* **14**, 3077; DOI:
777 10.1038/s41467-023-38755-4.

778 Tiklová K, Senti K-A, Wang S, Gräslund A & Samakovlis C (2010). Epithelial septate
779 junction assembly relies on melanotransferrin iron binding and endocytosis in Drosophila,
780 *Nat Cell Biol* **12**, 1071–1077; DOI: 10.1038/ncb2111.

781 Tu H-Y, Yuan B-S, Hou X-O, Zhang X-J, Pei C-S, Ma Y-T, Yang Y-P, Fan Y, Qin Z-H &
782 Liu C-F, et al. (2021). α-synuclein suppresses microglial autophagy and promotes
783 neurodegeneration in a mouse model of Parkinson's disease, *Aging Cell* **20**, e13522; DOI:
784 10.1111/acel.13522.

785 Vanden Broeck L, Naval-Sánchez M, Adachi Y, Diaper D, Dourlen P, Chapuis J, Kleinberger
786 G, Gistelinck M, Van Broeckhoven C & Lambert J-C, et al. (2013). TDP-43 loss-of-

function causes neuronal loss due to defective steroid receptor-mediated gene program switching in Drosophila, *Cell Rep* **3**, 160–172; DOI: 10.1016/j.celrep.2012.12.014.

Wang C, Liu Z & Huang X (2012). Rab32 is important for autophagy and lipid storage in Drosophila, *PLoS ONE* **7**, e32086; DOI: 10.1371/journal.pone.0032086.

Wang T, Guo H, Xiong B, Stessman HAF, Wu H, Coe BP, Turner TN, Liu Y, Zhao W & Hoekzema K, et al. (2016). De novo genic mutations among a Chinese autism spectrum disorder cohort, *Nat Commun* **7**, 13316; DOI: 10.1038/ncomms13316.

Winkler B, Funke D, Benmimoun B, Spéder P, Rey S, Logan MA & Klämbt C (2021). Brain inflammation triggers macrophage invasion across the blood-brain barrier in Drosophila during pupal stages, *Sci Adv* **7**, eabh0050; DOI: 10.1126/sciadv.abh0050.

Wu X & Tu BP (2011). Selective regulation of autophagy by the Iml1-Npr2-Npr3 complex in the absence of nitrogen starvation, *Mol Biol Cell* **22**, 4124–4133; DOI: 10.1091/mbc.E11-06-0525.

Xiong WC, Okano H, Patel NH, Blendy JA & Montell C (1994). repo encodes a glial-specific homeo domain protein required in the Drosophila nervous system, *Genes Dev* **8**, 981–994; DOI: 10.1101/gad.8.8.981.

Yang M, Wang H, Chen C, Zhang S, Wang M, Senapati B, Li S, Yi S, Wang L & Zhang M, et al. (2021). Glia-derived temporal signals orchestrate neurogenesis in the Drosophila mushroom body, *Proc Natl Acad Sci U S A* **118**; DOI: 10.1073/pnas.2020098118.

807 **Figures**

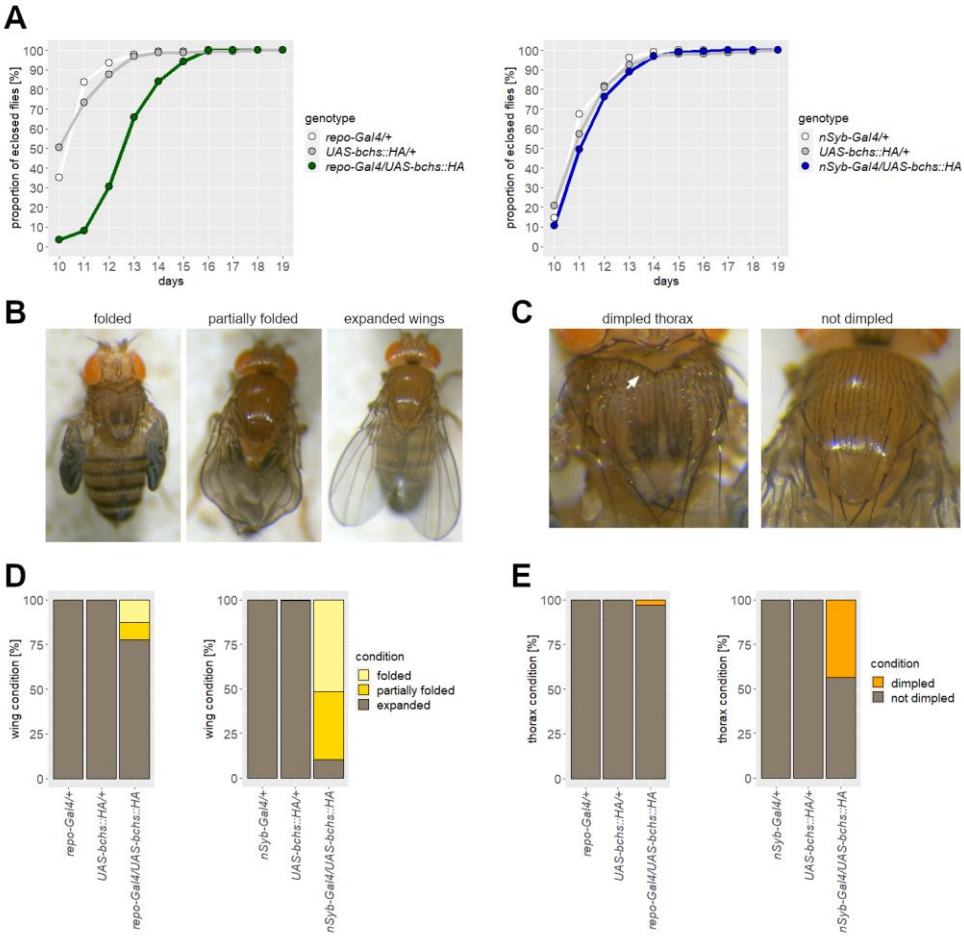

808

809 **Fig 1**. ***Developmental deficits in Bchs overexpression flies.***

810 A) Glial *Bchs* overexpression (left, *repo-Gal4/UAS-bchs::HA*, green) prolonged the
811 developmental time from egg to eclosion of adult flies, unlike neuronal overexpression (right,
812 *nSyb-Gal4/UAS-bchs::HA*, blue), in comparison to controls (left: *repo-Gal4/+* white, *UAS-*
813 *bchs::HA/+* gray) (right: *nSyb-Gal4/+* white, *UAS-bchs::HA/+* gray). Flies of 5 vials were
814 pooled. n > 88. B, C) Images of flies overexpressing *Bchs* in neurons. *Bchs* overexpression
815 caused wing expansion and dimpled thorax defects (arrow). D, E) Quantification of wing (D)
816 and thorax (E) defects. Both defects had a higher rate in neuronal than in glial *Bchs*
817 overexpression. n > 72.

818

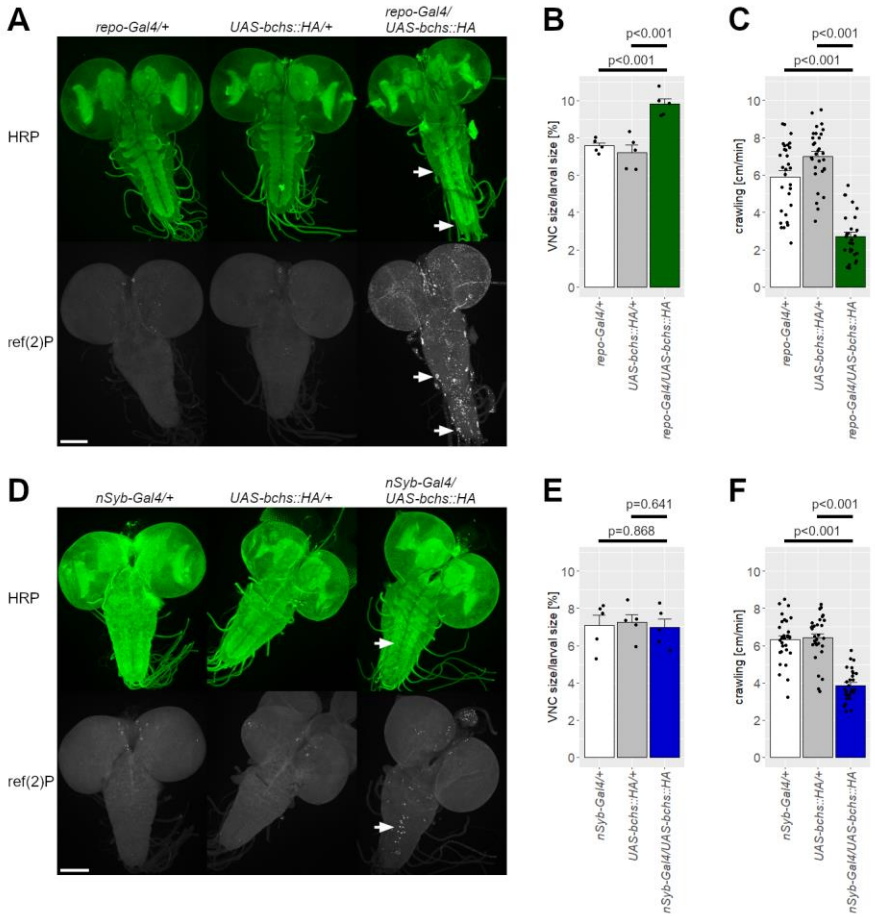

Fig 2. ***Larval locomotion and VNC length were affected by glial Bchs overexpression.***

A, D) Larval brains were stained against HRP (top) and ref(2)P (bottom). *Bchs* overexpression in glial cells (A, *repo-Gal4/UAS-bchs::HA,* right) and neurons (D, *nSyb-Gal4/UAS-bchs::HA,* right) caused accumulation of ref(2)P, in contrast to controls. Arrows exemplary point out ref(2)P aggregates. Scale bar: 100 µm. B, E) Quantification of VNC length normalized to larval length. Increased VNC length was observed in glial *Bchs* overexpression (B, green) larvae but not neuronal overexpression (E, blue). n =5. C, F) Overexpression of *Bchs* in glial cells (C, green) or neurons (F, blue) reduced the crawling velocity. n > 29. B, C, E, F) Data are shown as mean ± SEM.

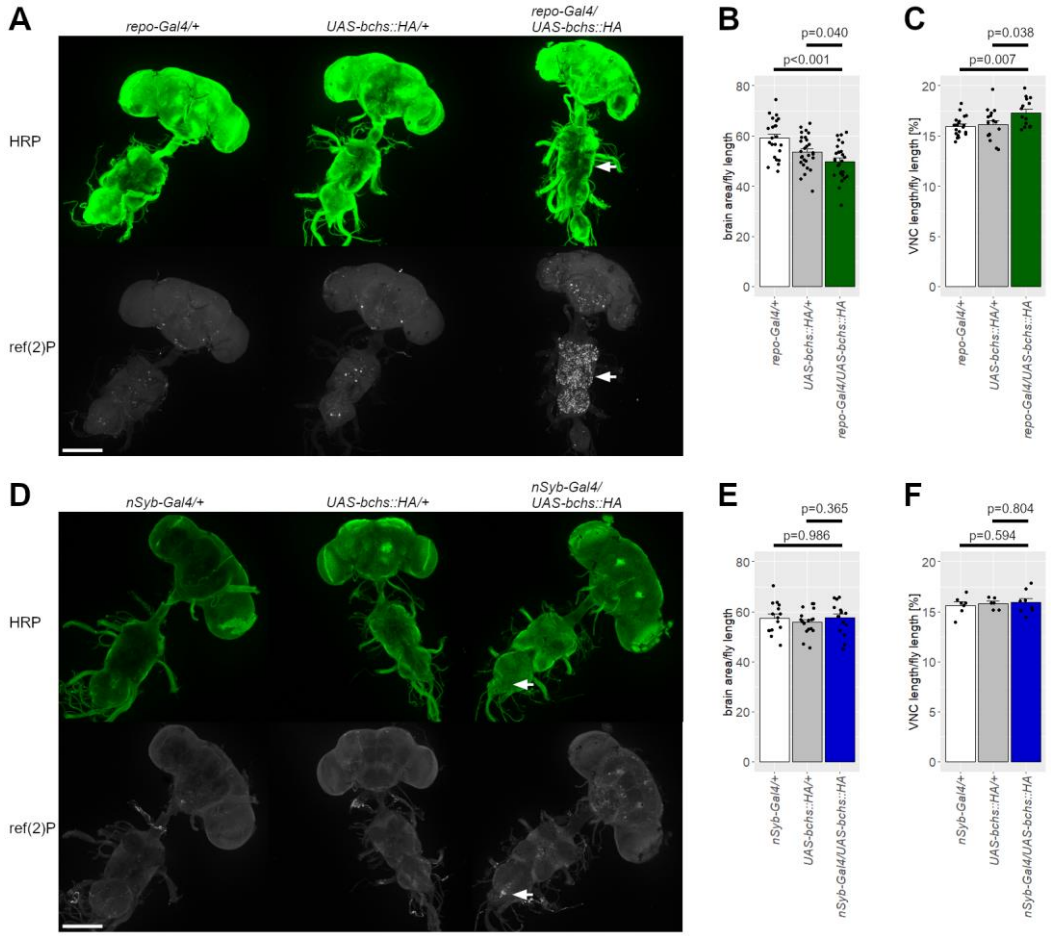

Fig 3. ***Glial Bchs overexpression affected adult CNS size.***

A, D) Adult CNSs were stained against HRP (top) and ref(2)P (bottom). *Bchs* overexpression in glial cells (A, *repo-Gal4/UAS-bchs::HA,* right) caused accumulation of ref(2)P in the brain and thoracic neuromeres of the VNC. Neuronal *Bchs* overexpression (D, *nSyb-Gal4/UAS-bchs::HA,* right) led to ref(2)P accumulation in the brain and posterior region of the VNC. Arrows indicate ref(2)P accumulation. Scale bar: 200 µm. B, E) Quantification of brain size normalized to fly length. A decreased brain size to fly length ratio was noted in glial *Bchs* overexpression adults (B, green) but not for neuronal overexpression (E, blue). B) $n \geq 23$. E) $n \geq 15$. C, F) Overexpression of *Bchs* in glial cells (C, green), but not in neurons (F, blue), elongated the VNC length (normalized to fly length). C) $n \geq 15$. F) $n \geq 6$. B, C, E, F) Data are shown as mean ± SEM.

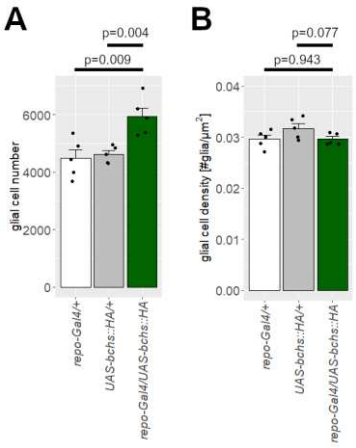

Fig 4. ***Glial cell number in larval CNS increased by glial Bchs overexpression.***

A) Glial nuclei in the larval CNS were counted by staining against repo. B) Glial cell density was determined by dividing the glial cell number by the larval CNS area. A, B) Glial *Bchs* overexpression raised the glial cell number but did not alter the glial cell density. n = 5. Data are shown as mean ± SEM.

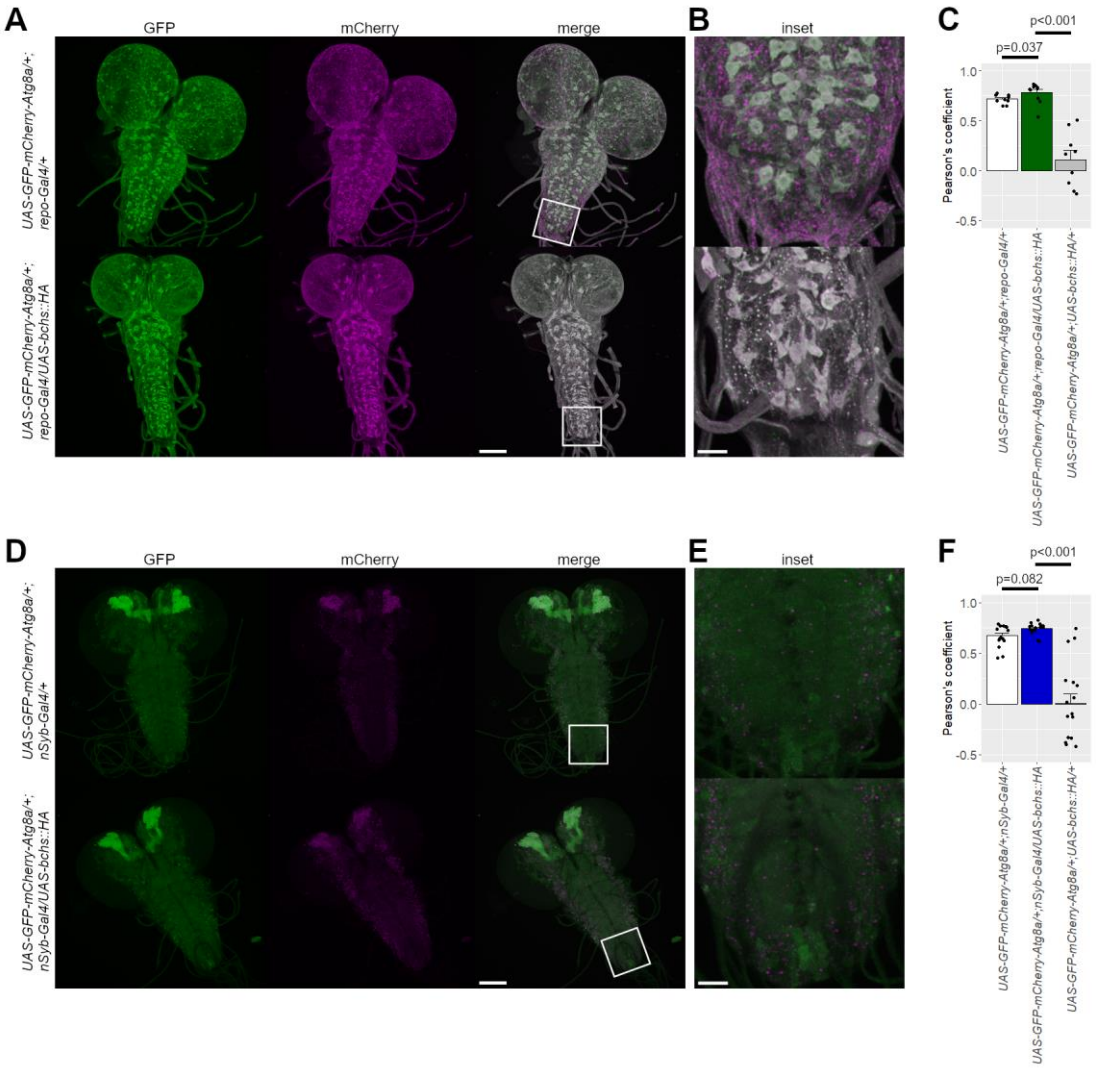

Fig 5. ***Ratio of non-acidic to acidic autophagic vesicles was altered through Bchs overexpression.***

A−F) The GFP-mCherry-Atg8a reporter was used to investigate autophagic flux in larval brains and was expressed in the same cell type as the *Bchs* overexpression. Autophagic flux was compared between larvae only expressing the Atg8a reporter (top, white, A−C: *UAS-GFP-mCherry-Atg8a/+; repo-Gal4/+* and D−F: *UAS-GFP-mCherry-Atg8a/+; nSyb-Gal4/+*) and larvae expressing the Atg8a reporter simultaneously with the *Bchs* overexpression (A−C: bottom, green, *UAS-GFP-mCherry-Atg8a/+; repo-Gal4/UAS-bchs::HA* and D−F: bottom, blue, *UAS-GFP-mCherry-Atg8a/+; nSyb-Gal4/UAS-bchs::HA*). As negative controls animals were used which carried both *UAS*-target genes, but not the *Gal4* (C, F: gray, *UAS-GFP-*

mCherry-Atg8a/+; UAS-bchs::HA/+, Fig S9). A, D) GFP (left) and mCherry (middle) signals were imaged with a confocal microscope and images were deconvoluted. Right: GFP and mCherry images merged. Scale bar: 100 µm. Box indicates the region of the insets shown in (B) and (E). B, E) Scale bar: 20 µm. C, F) Quantification of colocalization of GFP and mCherry signals using Pearson's coefficient. C) $n \geq 9$. F) $n \geq 16$. Data are shown as mean ± SEM.